JOURNAL OF GEOPHYSICAL RESEARCH, VOL. 112, B09303, doi:10.1029/2006JB004612, 2007

Effects of mesoscopic-scale fault structure on dynamic earthquake ruptures: Dynamic formation of geometrical complexity of earthquake faults

Ryosuke Ando[1,2] and Teruo Yamashita[3]

Received 3 July 2006; revised 28 February 2007; accepted 1 June 2007; published 12 September 2007.

[1] We develop a new hierarchical earthquake rupture model that takes into account mesoscopic-scale fault structure; shear branches nucleated on the main fault are specifically assumed as an example of mesoscopic-scale fault structure. We numerically investigate dynamic formation of fault geometry and its effects on dynamic earthquake rupture process based on this rupture model. As long as the length of the main fault is below a certain threshold L_{m}, the growth of these branches is shown to be arrested spontaneously soon after their nucleation. The spatial distribution of arrested branches is shown to form a self-similar geometrical structure. This suggests the existence of a simple scaling relationship between small and large events as long as the length of the main fault is below the threshold L_m. However, once the length of the main fault exceeds L_m, a limited number of branches begin unstable growth, and their sizes soon become comparable to that of the main fault. In other words, mesoscopic-scale branches are spontaneously transformed into macroscopic-scale ones. This finding indicates the critical importance of the consideration of mesoscopic-scale fault structure in understanding rupture dynamics: Once macroscopic-scale branches are formed, they change the fault geometry, which will considerably affect the rupture dynamics. The emergence of macroscopic branches suggests that the above mentioned simple scaling relation is never valid above a critical length L_m. Our study thus indicates that relationship between small and large earthquakes is complicated by the spontaneous transformation of a mesoscopic-scale fault structure into a macroscopic-scale one.

Citation: Ando, R., and T. Yamashita (2007), Effects of mesoscopic-scale fault structure on dynamic earthquake ruptures: Dynamic formation of geometrical complexity of earthquake faults, *J. Geophys. Res.*, *112*, B09303, doi:10.1029/2006JB004612.

1. Introduction

1.1. Geometrical Complexity and Hierarchy Structure of Earthquake Fault

[2] Earthquakes are geometrically complex ruptures that span a wide spectrum of lengths. Since earthquake ruptures are generally regarded as highly nonlinear phenomena, a key may exist for the understanding of earthquake rupture dynamics even in small-scale ruptures that occur accompanying the main rupture on the principal fault plane. The existence of such small-scale ruptures is well known. In fact, a natural fault is known to consist of a hierarchical structure ranging from the scale of fine grains forming a gouge or ultracataclasite zone along the principal slip plane (Figure 1, top) up to that of fault system consisting of discrete fault segments (Figure 1, bottom) and/or branched fault segments (Figure 1, middle and bottom) [e.g., *Chester and Kirschner*, 2000; *Di Toro et al.*, 2005; *Kim et al.*, 2004]. Since the mechanisms of nucleation, propagation and termination of dynamic earthquake ruptures ought to be defined by a physical process in the above physical entity, the assumption of a planar single fault, which is generally the case in many earthquake source studies, will not be reasonable for the modeling of earthquake rupture dynamics.

[3] *Moore and Lockner* [1995] conducted laboratory experiments on shear rupture and found that tensile microcracks are evident around the tips of relatively large shear cracks. The tensile cracks they observe are up to grain size. *Vermilye and Scholz* [1998] also found tensile microcracks around exhumed faults. These tensile microcracks are known to form a damage zone near the principal slip plane. Shear branches, which are much larger than these tensile microcracks, are also found widely in the field, and their lengths are know to span a wide spectrum of lengths from scales much smaller than total lengths of faults [*Sowers et al.*, 1994; *Tchalenko and Berberian*, 1975; *Vermilye and Scholz*, 1998] to scales comparable to them [*Archuleta*, 1984; *Fukuyama et al.*, 2003; *Nakanishi et al.*, 2002; *Sowers et al.*, 1994].

[1]Department of Earth and Planetary Science, University of Tokyo, Tokyo, Japan.
[2]Now at National Research Institute for Earth Science and Disaster Prevention, Tsukuba, Japan.
[3]Earthquake Research Institute, University of Tokyo, Tokyo, Japan.

0148-0227/07/2006JB004612$09.00

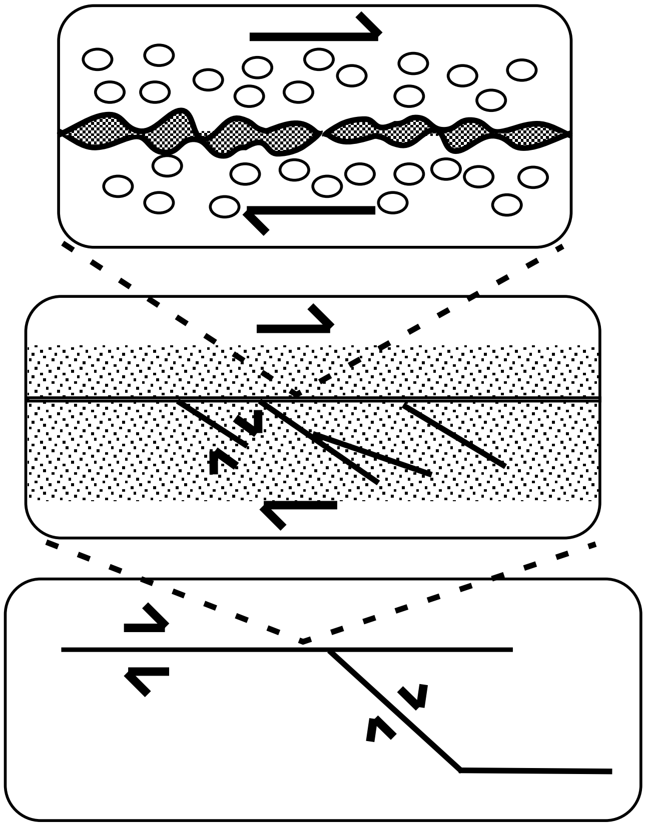

Figure 1. Schematic illustration of hierarchical structure of earthquake fault. (bottom) Scale of entire length of a fault system composed of planar segments (macroscopic-scale), (middle) length scale of fault zone involving damage zone (shaded) and branches (mesoscopic-scale), and (top) scale of frictional surface involving gouge and microcracks (microscopic-scale).

[4] The above stated shear branches and damage zone are considered to be created by a large dynamic stress change due to the passage of rupture fronts [*Andrews*, 1976a, 2005; *Poliakov et al.*, 2002; *Rice et al.*, 2005; *Scholz et al.*, 1993]. The formation of fault damage zone due to the dynamic extension of two-dimensional (2-D) mode II fault tips is actually modeled in some theoretical studies [*Andrews*, 2005; *Lyakhovsky et al.*, 1997; *Yamashita*, 2000] assuming dynamic effects of extending fault tips. A similar 3-D simulation is also made by a discrete element method [*Dalguer et al.*, 2003]. Formation of an approximately self-similar shaped fault damage zone, which has a triangular shape, is a common feature observed in the above theoretical studies [*Andrews*, 2005; *Ben-Zion and Shi*, 2005; *Dalguer et al.*, 2003; *Yamashita*, 2000].

[5] On the other hand, the formation of shear branches, which are also a major element forming the fault structure, and its effects on the dynamic earthquake rupture are poorly investigated. Formation of shear branches is implied by analytically evaluated stress distributions around the dynamically extending tip of a semi-infinite shear crack [*Poliakov et al.*, 2002] and finite slip pulse [*Rice et al.*, 2005]. In fact, *Kame and Yamashita* [1999a, 1999b] showed numerically that a front of rupture in an intact elastic medium is bifurcated spontaneously when the extending velocity exceeds a certain threshold. *Kame et al.* [2003] investigated the selectivity of rupture paths on a preexisting fault with a single bifurcation. However, they did not take into account the spontaneous multiple bifurcation; the interactions between shear branches will play an important role in the fault dynamics if a large number of branches are excited and the distribution density is high enough.

1.2. Fundamental Problems in the Prevailing View About the Modeling of Earthquake Ruptures

[6] An earthquake is commonly modeled as shear rupture on a thin fault plane in an elastic medium obeying some fault constitutive law, which is derived empirically based on laboratory experiments [e.g., *Marone*, 1998; *Ohnaka*, 2003]. The values of model parameters in the fault constitutive law relevant to natural earthquakes are estimated mainly in seismic wave inversion analyses. For example, dynamic modeling of the 1992 Landers, California, earthquake appears to have successfully reproduced both seismologically inverted slip history and observed seismograms in the frequency range up to about 1 Hz assuming a simplified slip-weakening law on a planar fault [*Olsen et al.*, 1997; *Peyrat et al.*, 2001] or a nonplanar fault system schematically shown in Figure 1 (bottom) [*Aochi and Fukuyama*, 2002].

[7] However, it is still a fundamental problem that laboratory-derived constitutive friction laws are applied directly in modeling based on seismic wave inversion analyses; note that length scales supposed in the laboratory experiments are significantly smaller than those in the seismic wave inversion analyses. While small samples only up to 10^{-1} m [e.g., *Scholz*, 2002] are generally employed in the laboratory experiments, spatial resolutions of the seismic wave inversions are about a few km at most in the direction along a fault and zero in the fault normal direction [e.g., *Ide and Takeo*, 1997] due to the band limited nature of seismic wave data, relatively small numbers of observation stations, uncertainty of seismic velocity structure and so on.

[8] In addition to the above scale problem, restrictions in laboratory experiments make the application to natural earthquakes also difficult. For example, many experiments have employed precut samples with nominally flat fault surfaces[e.g., *Dieterich and Kilgore*, 1994; *Ohnaka and Kuwahara*, 1990]; the hierarchical fault structure observed in nature is not taken into account. Even if the fault structure is considered, it is simulated only as a simple thin layer filled with gouge particles [e.g., *Marone*, 1998] in contrast to the hierarchical structure observed in the field. It is also a problem that stress and displacement are measured away from the fault along a loading axis [e.g., *Marone*, 1998] in many laboratory experiments, which implies that the measured quantities are ones averaged over the entire sample. In addition, dynamic fault propagation inside a sample cannot be traced in such measurements, while the detailed observation of spatiotemporal dynamic fault growth is fundamental to understand what control the earthquake dynamics. Although fault tip propagation is traced in some experiments by measuring the strain at some points along a fault in rocks [*Ohnaka and Kuwahara*, 1990] or recently in polymeric materials [*Xia et al.*, 2004], precut nominally flat

planes are assumed to model the fault; hierarchical fault structure is not properly simulated in these experiments.

1.3. Basic Concept of the Present Study: Introduction of Mesoscopic-Scale Fault Structure

[9] We have to detail the concept of spatial scales to take account of hierarchical fault structure in our modeling. While the concept of macroscopic and microscopic length scales is sometimes employed in earthquake source studies, they are mentioned in different ways according to authors [e.g., *Kanamori and Heaton*, 2000; *Marone*, 1998; *Ohnaka*, 2003]. For example, the macroscopic length scale usually refers to the size of samples in laboratory experiments, while the microscopic length scale could be used to refer to any objects of smaller sizes such as fault gouge particles, real contact areas or tensile cracks between grains. For the analysis of natural earthquakes, while the macroscopic length scale usually refers to the total fault length, the microscopic length scale could be employed for any objects of smaller sizes such as subfaults assumed in seismic wave inversion analyses, or branch faults or fault zone widths observed in field studies.

[10] It is, however, crucially important in the modeling study how microscopic and macroscopic length scales are defined since physical phenomena are ignored in the modeling if their typical length scales are smaller than the microscopic one; only their gross property is taken into account if their typical length scales are greater than the macroscopic one. If we consider only the microscopic and macroscopic length scales in the modeling, we may lose physically important properties between them. To address this problem, we here introduce the concept of mesoscopic length scale. Note that we do not argue that the consideration of the three length scales, microscopic, mesoscopic, and macroscopic scales, is sufficient for the modeling of dynamic earthquake ruptures. We rather point out in this paper that a new and deeper understanding can be acquired on the earthquake rupture dynamics by introducing this new length scale.

1.4. Aim and Outline of the Present Study

[11] We will propose a conceptually new model in this and following papers from the above viewpoint. A key element in our modeling is the explicit introduction of hierarchical fault structure; we particularly consider the spontaneous growth of secondary shear branches. These secondary branches introduce a mesoscopic-scale fault structure in our model: this mesoscopic-scale structure bridges the microscopic and macroscopic-scale ones observed in laboratory experiments and seismic wave inversion analyses.

[12] We will show below that mesoscopic-scale shear branches cease to extend soon after their nucleation and form an approximately self-similar geometrical structure if the extension distance of the main fault is below a certain threshold. Once the extension distance of main fault tip exceeds the threshold, a limited number of branches begin unstable growths; their sizes soon become comparable to that of the main fault. This indicates that simple scaling does not exist in geometrical properties of earthquake faults. We will show that the onset of this unstable growth is largely due to strong nonlinear interactions between the shear branches and to the stress enhancement caused by the extension of the main fault. The breaking of simple scaling relationship was never observed when the mesoscopic-scale fault structure is treated as a bulk continuous zone [*Andrews*, 2005; *Ben-Zion and Shi*, 2005; *Dalguer et al.*, 2003; *Yamashita*, 2000]. The dynamic branching of rupture paths found associated with earthquakes [e.g., *Sowers et al.*, 1994] might be related to this breaking.

2. Model

2.1. Definition of Mesoscopic Scale Characterizing Fault Structures

[13] For clarification, we conceptually define the length scales as follows: The microscopic length scale is defined to be much smaller than sizes of laboratory samples that are up to a few m. As shown in Figure 1 (top), phenomena of the microscopic length scale are observable in laboratory experiments such as the change of real contact area [*Dieterich and Kilgore*, 1994], rotation or displacement of fault gouge particles [*Marone et al.*, 1990] and tensile microcracking [*Moore and Lockner*, 1995]. The mesoscopic length scale is defined to be much smaller than an entire fault length, but larger than the above microscopic length scale (Figure 1, middle). Constitutive friction laws formulated based on laboratory experiments such as a slip-weakening law [*Ohnaka*, 2003] or a rate- and state-dependent law [*Ruina*, 1983] are considered to be some representation of microscopic processes averaged over the mesoscopic scale length corresponding to the sample size in this case. The dynamic process of phenomena having mesoscopic length scale is difficult to observe directly and only the resulting macroscopic phenomena can be observed by field observations or seismic wave inversion analyses. We can mention branches, bends and step overs as typical fault structures having mesoscopic length scales according to our definition, which may play a crucial role in the dynamics of fault. The macroscopic length scale is defined to be a scale comparable to the whole fault length (Figure 1, bottom). Phenomena of this scale can be estimated by seismic wave inversion analyses in terms of fault slip and stress drop. Since earthquakes occur over wide range of magnitudes, the definition of the macroscopic scale might be relative. What is important here is to try to understand macroscopic fault phenomena via the introduction of mesoscopic length scale. It will be shown in this paper that this gives a new perspective for the understanding of dynamics of earthquake ruptures.

2.2. Boundary Integral Equation Method

[14] We employ an elastodynamic boundary integral equation method(BIEM) [*Cochard and Madariaga*, 1994; *Tada and Madariaga*, 2001; *Tada and Yamashita*, 1997] for the simulation of dynamic growth of fault with branches in a 2-D infinite, homogeneous and isotropic elastic medium on which a uniform load is applied at infinity. We consider mode II ruptures, where the opening of the fault is prohibited. The BIEM has advantages in an accurate treatment of nonplanar faults and growth of their tips on self-chosen paths [*Ando*, 2005; *Ando et al.*, 2007, 2004; *Kame and Yamashita*, 1999a, 2003].

[15] Generally, in the 2-D BIEM, the change in the stress tensor σ on the fault can be described in terms of fault slip rate in the discretized form:

$$\boldsymbol{\sigma}^{i,n} = -\frac{\mu}{2\beta}V^{i,n} + \sum_j \sum_m K^{i,n,n-m}V^{j,m} \tag{1}$$

at the ith spatial node and nth time step, where $V^{\mathrm{j,m}}$ is the fault slip rate at the jth spatial node and mth time step, μ is the shear modulus, β is the S wave speed and K is the convolution kernel [e.g., *Ando et al.*, 2004]. We can obtain the slip rate V by numerically solving the integral equation (1) if the traction T is given, or expressed as a function of slip or slip rate on the fault. The stress generated by the growth of fault can be calculated from equation (1) once the slip rate is obtained.

2.3. Slip-Weakening Friction Law

[16] We assume a slip-weakening friction law, observed in a variety of laboratory experiments [*Dieterich*, 1979; *Marone*, 1998; *Ohnaka and Kuwahara*, 1990] for the analysis of slip on fault segments, which make up a fault system. Note that it will generally be more reasonable to apply laboratory derived microscopic laws to each segment of fault system than directly to a macroscopic planar fault, which is a macroscopic representation of geometrically complex fault system. For the numerical treatment below, we employ a simple linearized slip-weakening law often used in previous studies [e.g., *Ida*, 1972; *Kame et al.*, 2003]:

$$\tau(S) = \frac{(\tau_p - \tau_r)}{D_c}(D_c - S)H(D_c - S) + \tau_p, \tag{2}$$

where τ_p, τ_r, S, D_c and $H()$ denote the peak shear strength, residual shear strength, slip, critical slip displacement and a unit step function, respectively. For simplification, unless otherwise noted, we neglect the effect of normal stress on the above parameters; therefore τ_p and τ_r are assumed to be constant to represent the effect of cohesion; the effect of normal stress is taken into account only in the assumption of nucleation sites of branches as will be described below. This simplification is introduced because the effect of the normal stress on the fracture criterion has not been characterized well for the case we consider in this study, in which a rupture front dynamically propagates into a medium absent of any planes of weakness. In this case, the effect of cohesion could dominate that of the normal stress. However, from purely a theoretical view point, the normal stress effect assuming Coulomb friction will be examined and discussed in the section 7.1.

[17] The set of parameters in the slip-weakening law (2) determines characteristic spatial length scales. One of them is the critical nucleation length L_c; the slipping region grows stably under increasing load until finally the length L_c is reached, at which no further quasi-static solution exists for additional increase of the loading. We have the relation

$$L_c = \frac{16\mu}{3\pi}\frac{G_c}{(\tau_o - \tau_r)^2} \tag{3}$$

[*Aki and Richards*, 2002, p. 588, equation (11.83)] when Poisson's ratio is assumed to be 0.25, where τ_0 is the shear stress acting on the fault immediately before the appearance of fault and $G_c = (\tau_p - \tau_r)D_c/2$ denotes the fracture energy. We employ L_c as the normalization constant of the spatial length scale in the following analysis. The other important parameter is the size of breakdown zone at the static limit R_o; the breakdown zone is defined as a zone over which the shear strength degrades transitionally from the peak strength τ_p to the residual strength τ_r. The breakdown zone is called the process zone or slip-weakening zone in some literatures. It is known that the breakdown zone size takes a maximum value

$$R_0 = \frac{3\pi}{8}\frac{\mu D_c}{\tau_p - \tau_r}. \tag{4}$$

at the static limit [e.g., *Palmer and Rice*, 1973; *Rice*, 1980] and is diminished when the fault tip velocity reaches the Rayleigh wave speed v_{Rayleigh}, which appears to be disadvantageous to reliable numerical calculations for high-speed ruptures. However, if the breakdown zone is expressed by 4 spatial elements at least, the resolution of numerical solution is known to be satisfactory [*Kame et al.*, 2003].

2.4. Modeling of Branch Fault Segments

[18] As mentioned above, natural earthquake faults are not necessarily expressed only by single thin planes but are accompanied by a number of smaller-size shear fault segments branching out from the thin main slip planes. We now investigate how such branching occurs and how branch fault segments affect the dynamic growth of the whole fault system. Branch fault segments, hereafter simply referred to as branches, are assumed to be nucleated at some discrete points on the main fault, which implies that the main fault is weak locally at these points. We simply assume for numerical simulations to be tractable that possible nucleation points of branches are equally spaced on the main fault; in other words, the possibility of branch nucleation is investigated only at these points. Each branch is assumed to be nucleated at each prescribed point on the main fault once the main fault tip passes there. We assume that branches are nucleated only on one side of the main fault where the deformation is extensional (Figure 2) as suggested by *Poliakov et al.* [2002] and *Rice et al.* [2005]. We employ the hoop shear maximization criterion for the growth of each branch [*Ando et al.*, 2004; *Kame and Yamashita*, 1999a, 1999b; *Koller et al.*, 1992]. In other words, each branch tip extends into the direction of the maximum shear traction if the shear traction exceeds the shear strength. However, the secondary bifurcation is not allowed for each of branch for simplicity. The main fault is assumed to extend straight since we focus our attention on the extension process of branches.

[19] A uniform stress state caused by the remotely applied compressive stresses σ_1 and σ_2 ($\sigma_1 < \sigma_2 < 0$) is assumed to be a reference state (Figure 2), and the relative change from this state is analyzed below. We have to assume the strength of fault and stress change due to faulting for the simulation of fault growth, but we do not yet have very accurate knowledge about these two quantities, so that we assume here a simple and idealized model. We assume τ_r = 0 on each fault segment to simplify the analysis, so that the stress

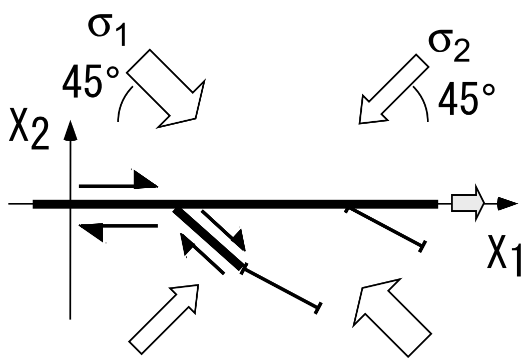

Figure 2. Configuration of our fault model. We assume the main fault along the x_1 axis, where the maximum stress drop occurs. Branches are assumed to be nucleated at prescribed points on the main fault soon after the passage of the tip of main fault there.

drop $\Delta\tau = \tau_o - \tau_r$ depends on the angle ϕ measured clockwise from the direction of x_1 axis in the form (see Figure 2)

$$\Delta\tau(\phi) = \tau_o(\phi) = \frac{\sigma_1 - \sigma_2}{2}\cos 2\varphi. \quad (5)$$

It will be reasonable to assume $\tau_r < \tau_o(0) < \tau_p$ on each fault segment immediately before the nucleation of dynamic faulting except at its nucleation zone. We specifically assume $\tau_o(0) = (\tau_p + \tau_r)/2$ in the following calculations, unless stated otherwise, taking the mean of the two values τ_p and τ_r, which implies that the strength excess $\tau_p - \tau_o$ is equal to the stress drop. The effect of Coulomb friction is examined in the section 7.1. We also assume $D_c/L_c = 2.0 \times 10^{-4}$ in the following calculations, unless stated otherwise, considering that the ratio of stress drop to shear modulus is known to be on the order of 10^{-3} in laboratory experiments [e.g., *Ohnaka*, 2003].

3. Stress Change Near the Extending Tip of a Planar Fault

[20] As will be shown, the growth of branches is triggered by significant stress change around the dynamically extending tip of the main fault. Hence it is useful for understanding the growth mechanism of branches to investigate the stress distribution around the extending tip of the main fault and its dependence on the extending velocity of the main fault.

[21] A planar main fault is assumed to appear suddenly over some length on the x_1 axis, which is slightly greater than the critical length L_c, and then its unilateral and spontaneous propagation is started in the positive direction of the x_1 axis. The slip-weakening friction law (2) is assumed on the fault. If the model parameters of the slip-weakening law are kept constant as assumed here, the fault tip extension is monotonically accelerated [*Andrews*, 1976b]. Figure 3 shows the spatial distribution of the ratio $\tau^{\max}/\tau_p$ around the extending fault tip at some instants, where $\tau^{\max}$ is the maximum shear traction given by $\tau^{\max} = \sqrt{(\sigma_{11} - \sigma_{22})^2/4 + \sigma_{12}^2}$, where σ_{ij} is the stress tensor component; only the area near the fault tip is illustrated here fixing the tip at the origin. Note that the shear traction is symmetric with respect to a fault plane contrasting with the asymmetric Coulomb stress patterns shown by *Poliakov et al.* [2002] and *Rice et al.* [2005]. Figure 3 clearly shows that branches are likely to begin their growths near the extending tip of the main fault; note that a zone where the ratio exceeds 1.0 (colored gray) potentially fails. It is also shown that the distance between the locations of peak of traction and fault tip tends to increase with rupture velocity. While the change of $\tau^{\max}$ at the immediate vicinity of fault tip is almost all due to the increase in σ_{12} with increasing fault length, that behind the fault tip is mainly due to the increase in $\sigma_{11} - \sigma_{22}$. It is worth emphasizing that the shear traction behind the fault tip may exceed the strength τ_p in the above numerical simulation since, while the shear traction is equated to τ_p at the extending fault tip, there is no constraint about the value of shear traction except at the fault tip. As shown in Figure 3, the direction of maximum shear traction tends to deviate from that of the x_1 axis behind the fault tip, which suggests the occurrence of branching out of the fault behind its tip of extension.

4. General Features of the Dynamic Fault Growth Process

[22] We first investigate general features of the dynamic growth process of a fault; a large number of branches are assumed to be nucleated on the main fault. Figure 4 shows snapshots of a typical example of fault growth. First, the main fault starts its extension and begins to nucleate branches. However, the nucleated branches do not begin their growths when the extension of the main fault is not large enough because of insufficient enhancement of stress (Figure 4a). As the size of the main fault increases, the shear stress is magnified near its extending tip and the stress enhancement zone expands as shown in Figure 3. If such stress enhancement becomes sufficiently large, branches can begin their growths while their extensions are arrested after attaining some lengths (Figures 4b and 4c). The spatial distribution of these arrested branches forms approximately a triangular zone on one side of the main fault. The lengths of these branches increase with increasing main fault size. As the main fault extends further and its size exceeds a certain critical length, a limited number of branches continue to grow together with the main fault without arresting. This suggests that complicated fault geometry can be generated dynamically. It is also shown in Figure 4 that the emergence of such large-scale branch tends to suppress the growth of the next nucleated branches in its neighborhood, which is due to the stress shadow effect as will be discussed below.

[23] Branches whose growths are arrested spontaneously and whose spatial distribution forms approximately a triangular zone are hereafter referred to as mesoscopic branches (mesobranches) in order to represent the feature that their sizes are much smaller than that of the main fault. Branches growing spontaneously to lengths comparable to that of the main fault are referred to as macroscopic branches (macrobranches). We will investigate below how the triangular zone appears for the spatial distribution of mesobranches and how a limited number of branches grow into macro-

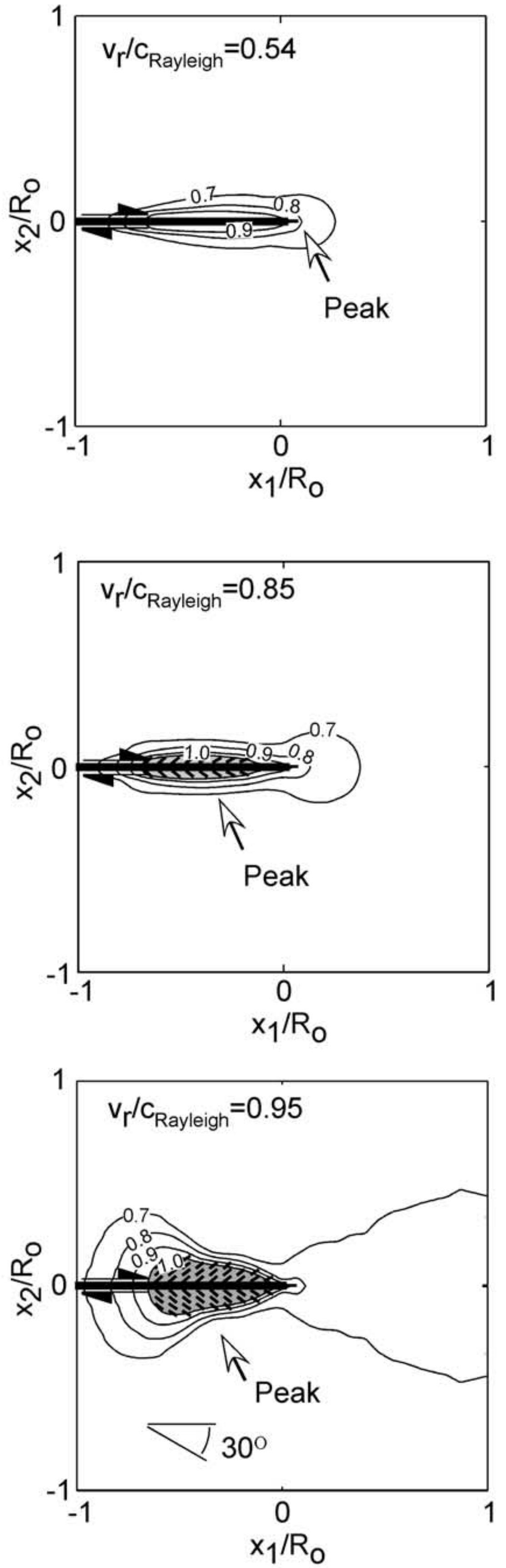

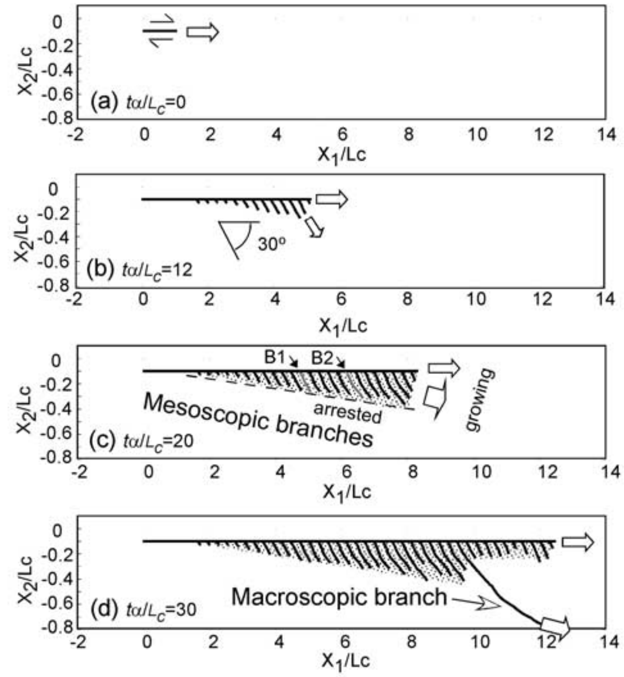

Figure 4. Snapshots of dynamic growth of fault with multiple branches. The value $\Delta B/L_c$ = 0.30 is assumed. Note that the scale is magnified in the x_2 direction. Shear traction change along the branches depicted by gray curves in Figure 4c is shown in Figure 5.

branches carrying out some additional calculations. However, the simulation of spontaneous growth of a large number of branches is very time consuming especially when their extending paths are determined by the hoop shear maximization criterion at each time step. We therefore fix the orientation of each branch at 30° in the following simulations except in some simulations focusing on the spontaneous growth of macrobranches: Figure 4, in fact, shows that the growth direction of each branch is approximately the same and makes an angle of 30° with the growth direction of the main fault as far as mesobranches are concerned.

5. Formation of Triangular Zone for the Spatial Distribution of Mesobranches

[24] We investigate the conspicuous phenomena observed in Figure 4 following the order of events in this and next sections. Let us begin with considering the formation mechanism of mesobranches for their triangular spatial

Figure 3. Spatial distributions of magnitude and orientation of maximum shear traction around the tip of fault at instants when the fault tip velocity attains the values $v_r/c_{\mathrm{Rayleigh}}$ = 0.54, 0.85, and 0.95. The isolines with interval 0.1 denote the ratio $\tau_{\max}/\tau_p$. The potential failure zone in which the shear traction exceeds the strength τ_p is shaded gray; the orientation of line segments denotes the direction of maximum shear traction.

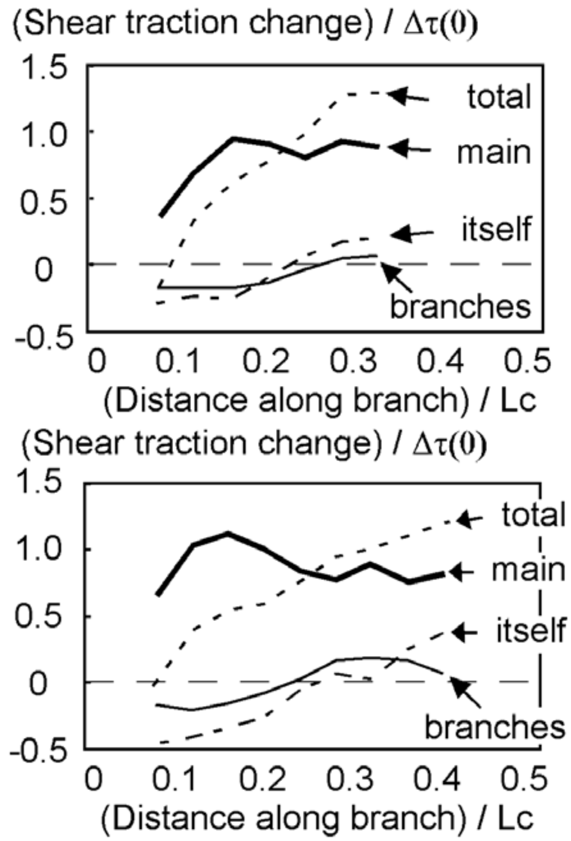

Figure 5. Shear traction change along two typical mesoscopic branches (top) B1 and (bottom) B2 shown in Figure 4c. $\Delta\tau(0)$ denotes the initial shear traction acting on the main fault plane (see equation (5)). The contributions from the main fault (main), the branch under consideration (itself) and the other branches (branches) are separately illustrated; the total shear traction change is given by a linear sum of these contributions. Each contribution is illustrated as a function of distance, along each branch, from its nucleation point at the instance when the branch extension is arrested.

distribution. Figure 5 illustrates the shear traction change along two typical mesobranches B1 and B2 shown in Figure 4c at the instants when these branches stop their extension; these two branches are collectively called branch B below because of the qualitative similarity in the behavior of traction change on the branches. We should first note that the growth of each branch ought to be affected by the stress state there. Since the traction change on branch B can be expressed as a linear sum of contributions from the main fault, branch B, and the other branches, these three contributions are separately illustrated. We find in Figure 5 that the contribution from the main fault is largest over branch B. The largest contribution occurs because the sizes of branches are negligibly small compared with that of the main fault. Figure 3 supports that the shear traction is enhanced significantly on a section of branch B that is in the stress enhancement zone formed near the extending tip of the main fault. This makes the contribution of the main fault largest at the nondimensional distance 0.15 ~ 0.20 on the branches B1 and B2. However, the tip of branch B gets out of the stress enhancement zone, which causes a decrease in the contribution of the main fault (Figures 5 and 6). This will decelerate the growth of branch B and finally arrest its extension. In other words, the branch stops extension because of the loss of enough driving force for the growth due to the enhanced stress near the tip of the main fault. Hence we can conclude from the above consideration that the size of arrested mesobranch is determined by the size of stress enhancement zone formed near the extending tip of the main fault. This conclusion suggests that the size of arrested mesobranch increases with the extension of the main fault, as actually observed in Figure 4, since the size of stress enhancement zone increases monotonically with the extension of the main fault.

[25] Next we should note that the extending velocity of the tip of the main fault soon attains a constant value with the extension (Figure 7). This will contribute to the formation of an approximately self-similar shape for the spatial distribution of mesobranches. In fact, a self-similar crack solution [*Kostrov*, 1964] indicates that the size of stress enhancement zone formed near the crack tip increases linearly with the crack length. Since the length of arrested mesobranch is largely determined by the size of stress enhancement zone as stated above, an approximately self-similar distribution is expected to be formed as soon as the extending velocity of the main fault attains a constant value as actually observed in Figure 4.

[26] Densely distributed mesobranches form a significantly deformed zone surrounding the main fault, so that the distribution zone of mesobranches (shadowed in Figures 4c–4d) may correspond to a fault zone observed for a natural fault. Hence the distribution zone of mesobranches is referred to as the fault zone in this paper. We observe an approximate linear relation between the fault zone width W_z and the length of the main fault L for $L < L_m$, where L_m

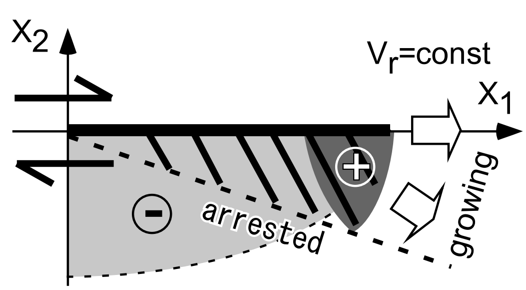

Figure 6. Schematic illustration of the generation mechanism of triangular zone for the spatial distribution of mesobranches. The dark gray zone denotes a zone where the shear traction is enhanced along mesobranches, while the light gray zone denotes a zone where the traction is reduced; only the contribution from the main fault is shown. The light gray zone is sometimes referred to as the stress shadow. The dimension of light and dark gray zones increases in proportion to the length of main fault when the fault tip velocity v_r is constant. The growth of branches is promoted in the dark gray zone, while their extensions are highly decelerated soon after they enter the light gray zone (stress shadow) as far as the length of the main fault is below a certain threshold (see also section 6).

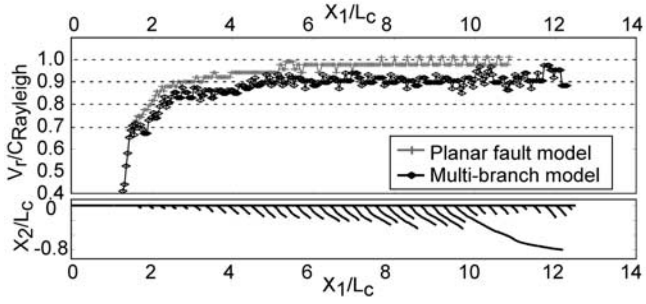

Figure 7. Sub-Rayleigh rupture velocity of main fault due to multiple branching. (top) Fault tip velocity (black curve) in the multibranch model corresponding to the case shown in Figure 4. Gray curve shows the case of planar fault model with no branches; the other assumptions are the same as in the multibranch model. (bottom) Corresponding fault (thick curves) geometry of the multibranch model.

is the length of the main fault at the instant when a macrobranch first appears:

$$W_z = AL \tag{6}$$

Here A is the proportionality coefficient, whose dependence on the model parameters will be investigated below; the fault zone with W_z is defined as the maximum width of fault zone at the instant when the main fault attains the length L (see Figure 8a). A linear relation between the width of damage zone and the length of the main fault is also found in numerical simulations of the formation of damage zone caused by the stress perturbation due to dynamic fault growth [*Andrews*, 2005; *Ben-Zion and Shi*, 2005; *Dalguer et al.*, 2003; *Yamashita*, 2000].

[27] Our model is characterized by the two length scales; one is the nondimensional spacing between two adjacent points of branch nucleation $\Delta B/L_c$ and the other is the nondimensional static breakdown zone size $R_o/L_c = 9\pi^2/64\{(\tau_o - \tau_r)/(\tau_p - \tau_r)\}^2$ (refer to equations (3) and (4)). If we assume the relation $\tau_o(0) = (\tau_p + \tau_o)/2$ (see section 2) as in Figures 4 and 7, R_0/L_c is reduced to a constant $9\pi^2/256$. We investigate in Figure 8 how the geometrical shape of fault zone is dependent on $\Delta B/L_c$ fixing R_0/L_c at $9\pi^2/256$. Figure 8 shows that the ratio $A = W_z/L$ increases with increasing $\Delta B/L_c$. This phenomenon can easily be understood because interactions between more densely distributed branches tend to impede their growths more; a smaller value of $\Delta B/L_c$ means a larger impediment to branch growth. We find that the dependence of the ratio W_z/L on $\Delta B/L_c$ is described approximately by a logarithmic function of $\Delta B/L_c$.

[28] We should now note that the dependence of $A = W_z/L$ on the breakdown zone size R_o/L_c is equivalent to the dependence on the inverse of square of the normalized breakdown stress drop, $(\tau_p - \tau_r)/(\tau_0 - \tau_r)^2$. Since earthquake main faults may in general have slipped repeatedly in their slip histories, the strength on the plane of main fault may be somewhat smaller than in the surrounding rock, which suggests that the strengths for branches are larger. We now investigate how such strength difference affects the geometry of fault resulting from the fault dynamics. Figure 9 shows the envelopes formed by connecting the arrested tips of the mesobranches for various values of the ratio R_0^b/R_0^m, where R_0^b and R_0^m denote the values of R_o/L_c on the branches and the main fault, respectively. We do not assume the relation $\tau_0 = (\tau_p + \tau_r)/2$ here and the value of τ_p is varied while τ_0 and τ_r are fixed at the values same as in all the other calculations. We observe that A decreases slightly as R_0^b/R_0^m increases if we compare the curves before the emergence of the macroscopic branches. This result is simply what we expect since branches tend to extend more

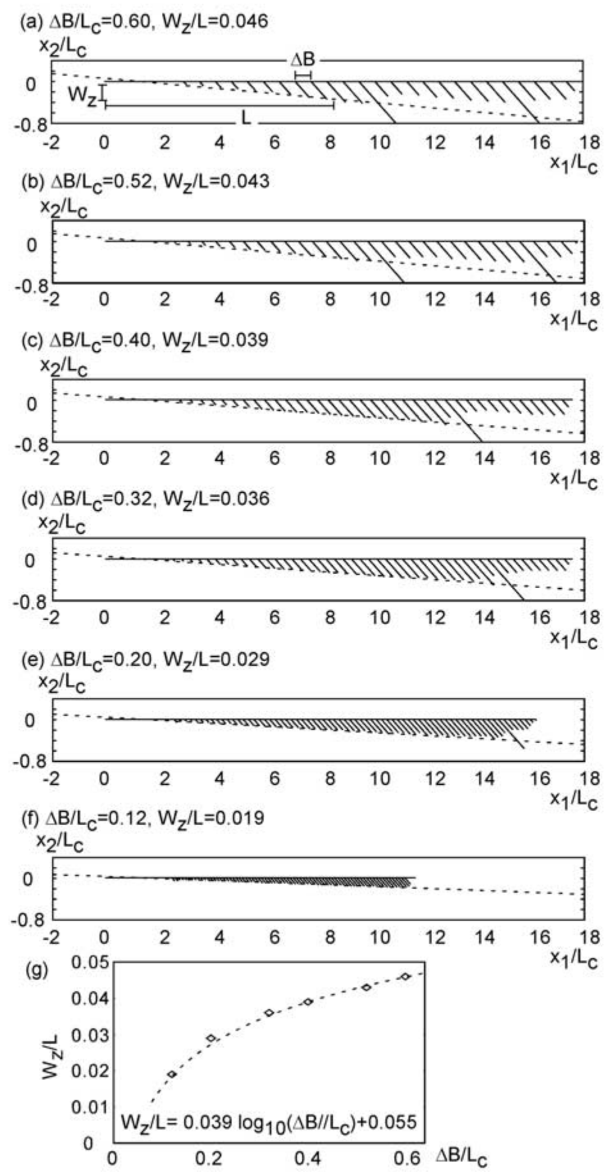

Figure 8. (a–f) Dependence of dynamically arisen fault geometry on the spacing between two adjacent points of branch nucleation. Fault segments arisen at certain instants are denoted by black lines. Dashed lines denote envelopes connecting the arrested tips of mesoscopic branches. The orientation of branches is fixed at 30° here. (g) Relation between fault zone width W_z/L and $\Delta B/L_c$.

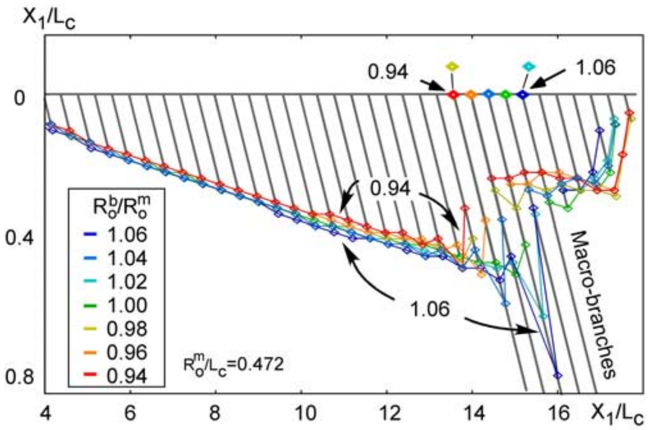

Figure 9. Dependence of the distribution of lengths of mesobranches on the value of R_0^b/R_0^m. The value shown in the inset is assumed for each colored curve. We assume the value $\Delta B/L_c = 0.40$ for all the examples shown here. The nucleation points of macrobranches are shown on the main fault with the diamonds.

in a material with lower strength (i.e., longer breakdown zone length). Just before the emergence of a macroscopic branch we clearly observed fluctuation in the lengths of mesobranches. The mechanism of fluctuation will be investigated below.

6. Emergence of Macrobranches

6.1. Effects of the Main Fault

[29] We know that the shear traction acting on a branch can be expressed as the linear sum:

$$\tau^{i,n} = \sum_j^{\Gamma_{main}+\Gamma_{self}+\Gamma_{branches}} \sum_m K^{i,j,n-m} V^{j,m}, \qquad (7)$$

where Γ_{main}, Γ_{self} and Γ_{branches} denote the contributions from the main fault, the branch now under consideration and the other branches, respectively. We first investigate the mechanism of emergence of macrobranches based on equation (7). The contribution from the main fault is shown in Figure 10a for three branches whose nucleation points are equally spaced on the main fault. Note that it was pointed out before that the main fault plays a dominant role in determining whether the growth of a branch is arrested or accelerated; its growth is promoted if it is in the stress enhancement zone formed near the extending tip of the main fault.

[30] In order to evaluate the stress increment driving the extension of branches, we specifically illustrate in Figure 10a the maximum value of shear traction taken, during the calculation, at each location on the three branches. The maximum value is found to be larger at locations nearer to the branch nucleation point in all the three examples, which suggests that a larger maximum value is taken at a location nearer to the extending tip of main fault. It is also found that the maximum value is larger along a branch formed later. This occurs because the stress is more enhanced at the tip of larger main fault (see Figure 6).

[31] Furthermore, first, one can observe that the contribution from the main fault is larger on the macrobranch than on the mesobranches. Second, as shown in Figure 6, the length of mesobranch is approximately equal to the size of the stress enhancement zone transiently formed near its nucleation point. Since the stress enhancement zone expands with the extension of the main fault, a branch tends to be larger with the extension of the main fault and the shear traction is more enhanced at the tip of the branch; hence the possibility of transformation into unstable growth increases. It is therefore suggested that the increase in the stress enhancement due to the extension of the main fault plays a critical role in the emergence of macrobranch. It is also suggested a branch growth is limited in the stress enhancement formed at the tip of the main fault preceding the stress shadow unless the branch length does not exceed a certain value, which is attained when the main fault reaches L_m. However, once its length exceeds this value, it can begin unstable extension.

[32] We should, however, note that it is not enough to understand yet how its growth is triggered and why only a limited number of branches grow into macroscopic ones; the above consideration has only focused on the interactions between the main fault and branches, and suggested the existence of minimum threshold length of the main fault for the emergence of macrobranch. These two can be explained from the viewpoint of interactions between branches as will be shown in section 6.2.

6.2. Fluctuation of Mesobranch Lengths

[33] Relation (6) suggests that the spatial distribution of mesobranches is approximately self-similar before the appearance of a macrobranch. However, the self-similarity tends to break down gradually. In fact, we observe fluctuation in the lengths of mesobranches some time before the emergence of macrobranch (Figure 9). The amplitude of fluctuation increases with the growth of the main fault and a macrobranch emerges after sharp increase in the fluctuation amplitude. This fluctuation provides us with a clue for

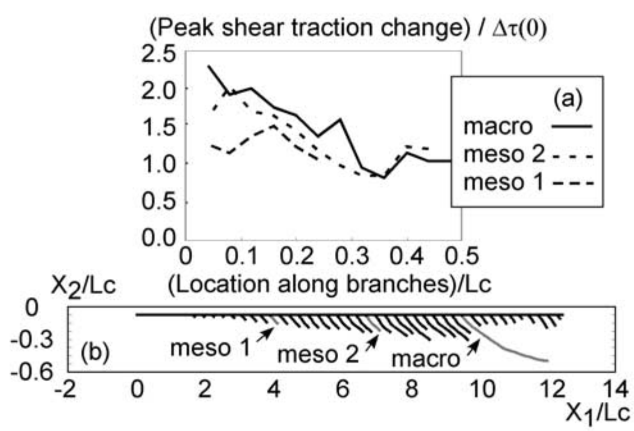

Figure 10. (a) Maximum value of shear traction change taken, during the calculation, at each location on the three branches. (b) Fault geometry. We assume the model same as in Figure 4 and carry out the calculation till the fault geometry illustrated in Figure 10b is formed. Only the contribution from main fault is illustrated here.

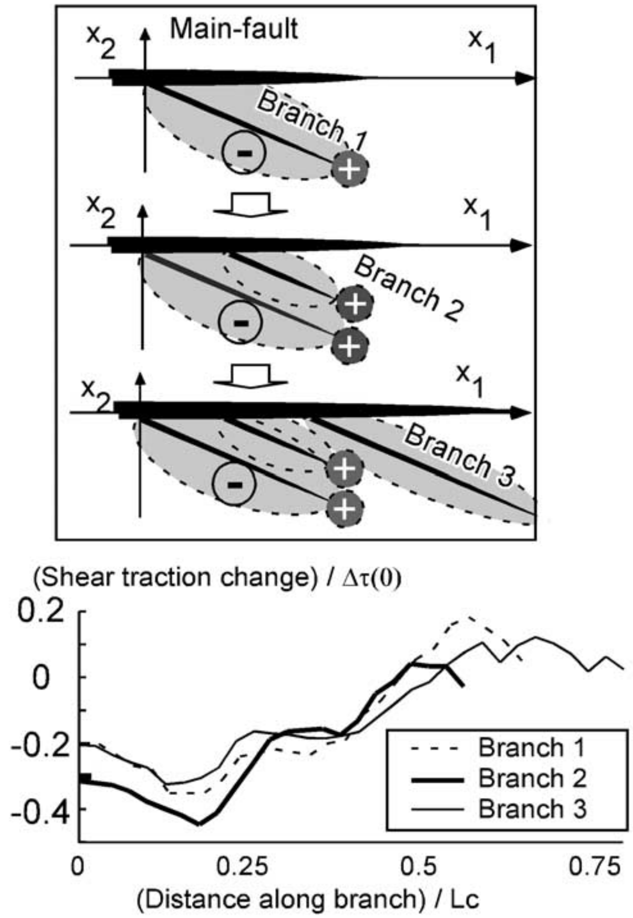

Figure 11. Mechanism of fluctuation in the lengths of branches. (top) Schematic illustration of the mechanism. The light and dark gray zones denote zones where the shear traction is largely released and enhanced due to the existence of branches, respectively. (bottom) Shear traction changes along three branches shown in Figure 9 in the case $R_0^b/R_0^m = 1$. $\Delta\tau(0)$ denotes the initial shear traction acting on the main fault plane (see equation (5)). Branch 3 corresponds to the macrobranch, and branches 1 and 2 correspond to the preceding two nearest mesobranches. The shear traction changes on branches 1 and 2 are the values taken at the instants when their growths are arrested. The value on branch 3 is taken at the instant when the fault geometry shown in Figure 9 is formed; since branches 1 and 2 are stationary at this instant, the shear traction changes on branches 1 and 2 at the instant when the fault geometry shown in Figure 9 are little different from those shown here. Note that the stress shadow effect is largest for branch 2, which has the shortest length.

understanding how their growths are triggered and why only a limited number of macrobranches emerge.

[34] The origin of this fluctuation will largely be attributable to nonlinear interactions between mesobranches and the discrete nature of our model as will be discussed now. First, we should note that a larger mesobranch casts a larger stress shadow in its neighborhood. Hence, if a mesobranch is grown larger than that expected from equation (6) by some heterogeneity, the length of next nucleated mesobranch will be smaller than expected from equation (6) because of the stress shadow cast by the former. Then the branch nucleated next to this smaller-size mesobranch tends to grow longer because a smaller-size crack generally causes a smaller stress shadow. In this way, the stress shadow effect causes the fluctuation in the lengths of branches; see Figure 11. The fluctuation amplitude rapidly increases with the growth of the main fault because each branch increases the possibility of unstable growth with the extension of the main fault (Figure 6) as stated above while the size of a stress shadow zone formed by each branch increases. These interactions between branches cause the fluctuation and a branch is eventually formed that is large enough for the unstable growth.

[35] Let us now discuss how the above mentioned extension of branch longer than expected from (6) occurs. This will be related to the discrete nature of our model. In our model, the tip of each branch can suddenly extend by a unit grid interval as soon as the fracture criterion is satisfied. Hence it is likely that slight numerical noise can cause a difference in the branch length by a unit grid interval even if the physical conditions are identical between each other. This has a little effect on fluctuation in the mesobranch lengths in an early phase of the growth of the main fault as observed in Figure 9. However, after mesobranches attain a certain length as a result of their lengthening (Figure 6), this slight fluctuation is amplified by the nonlinear interactions between mesobranches as stated above, and a few branches eventually begin unstable growth as shown in our simulation. In other words, our simulations show that the microscopic discreteness, which is much smaller than the sizes of mesobranches, affects the dynamic formation of macroscopic fault geometry through the nonlinear interactions between branches. Hence the possibility of application of our current fault model depends on whether nature has a property of discreteness at microscopic level; such discreteness implies strong microscopic heterogeneity. It is well known that an exhumed fault typically reveals a core of crushed rock bordered by a zone of damaged rock. This heterogeneous granular structure of fault will be better modeled by discreteness than continuity, so that it may be reasonable to

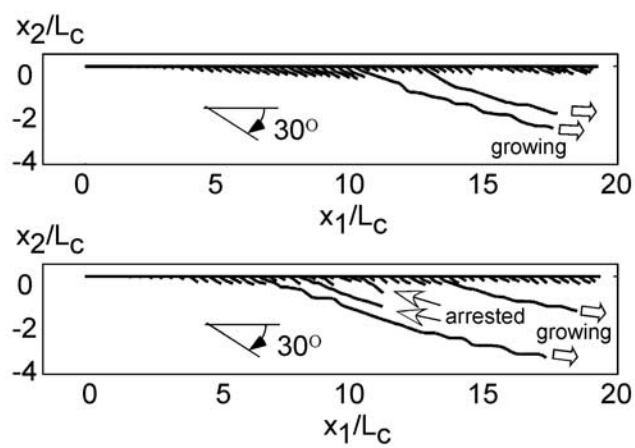

Figure 12. Examples of longer computation. We assume (top) $\Delta B/Lc = 0.31$ and (bottom) 0.38.

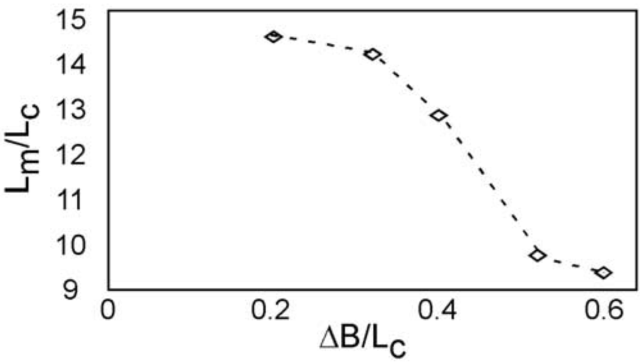

Figure 13. Relation between the nondimensional critical length of the main fault L_m and spacing between two adjacent nucleation points of branches ΔB. L_m is the length of the main fault at the instant when a macrobranch first appears.

introduce discreteness in modeling earthquake fault at the microscopic level. In addition, we should note that some authors have pointed out that the complex nature of earthquake statistics can be better simulated by discrete fault models [e.g., *Ben-Zion and Rice*, 1995; *Yamashita*, 1998].

6.3. Emergence of a Limited Number of Macrobranches

[36] Figure 12 shows two other examples of our simulations in which the hoop shear maximization criterion is assumed for the growth of each branch; the numerical computation is carried out much longer than in Figure 4. These examples clearly show that only a limited number of branches can grow into macrobranches. We now investigate how this occurs. A longer branch tends to suppress more the growth of the next nucleated branch as noted in section 6.2. Since the appearance of macrobranch casts especially large stress shadow in its neighborhood, the growths of subsequently nucleated branches will be highly suppressed as typically shown in Figure 12. Hence the main fault has to extend furthermore to trigger the growth of other macrobranches. This will explain the appearance of only a limited number of macrobranches.

6.4. Dependence of L_m on the Parameters ΔB and R_0

[37] We observed above that the critical fault length L_m is an important parameter in the analysis of dynamic of fault growth. We now investigate quantitatively the dependences of L_m on the characteristic length parameters $\Delta B/L_c$ and R_0/L_c. The relation between the critical length L_m/L_c and $\Delta B/L_c$ is illustrated in Figure 13, which is obtained in the simulation shown in Figure 8. As mentioned before, the growth of more densely distributed branches tend to be suppressed more, so that L_m/L_c should be larger for smaller ΔB as actually observed in Figure 13.

[38] Figure 14 shows the relation between the critical fault length L_m/L_c and breakdown zone size R_o^b/R_o^m, which is obtained in the simulation shown in Figure 9. Although some fluctuation is observed, we find that L_m/L_c tends to increase with increasing R_o^b/R_o^m. This result is physically reasonable in consideration of the ratio of the size of stress enhancement zone near the extending tip of the main fault to that of breakdown zone: larger stress enhancement zone is required for a branch with larger value of R_o^b/R_o^m to grow.

7. Discussion

7.1. Effects of Normal Stress

[39] Although we neglected the effects of normal stress on the friction in the above analysis, these effects are an interesting problem purely from a theoretical viewpoint. We now introduce a Coulomb friction model (CFM), and study the effect of normal stress in comparison with the normal stress-independent model (NIM) assumed above.

[40] In the Coulomb friction model, the peak and residual shear strengths are given by $\tau_p = \mu_s \times (-\sigma_n)$ and $\tau_r = \mu_d \times (-\sigma_n)$, respectively; normal stress is assumed to be negative for compression. While we assume that the peak strength is given by a linear sum of the initial static stress and dynamic stress, only the initial static stress is taken into account for the residual strength. This simplification is made because of the limitation of memory resource in our computer and necessity to keep the system size equivalent to the previous simulations; we can expect that this simplification does not make qualitative difference on results as will be discussed below.

[41] In CFM, the tips of branches are assumed to extend into the direction that maximizes the Coulomb stress $\mathrm{CFF}_s(\phi) = \tau - \tau_p = \tau + \mu_s \times \sigma_n$. We locate, in CFM, the main fault in the direction inclined by the angle $1/2 \times \tan^{-1}\mu_d$ from the direction of maximum initial shear stress, which maximizes the stress drop on the main fault; the clockwise rotation is assumed to give a negative angle. We assume $\mu_s = 0.6$ and $\mu_d = 0.12$ following *Kame et al.* [2003]. The stress drop $\tau_o - \tau_r$ and the breakdown stress drop $\tau_p - \tau_r$ on the main fault are kept equal between the two models of CFM and NIM by selecting appropriate values for the initial principle stresses.

[42] Figures 15a and 15b show snapshots of the fault geometry for CFM and NIM, respectively, obtained at the same time step ($t\alpha/\Delta s = 390$). First, we find in comparison between CFM and NIM that the lengths of mesobranches are generally larger in CFM. This is what we expect because

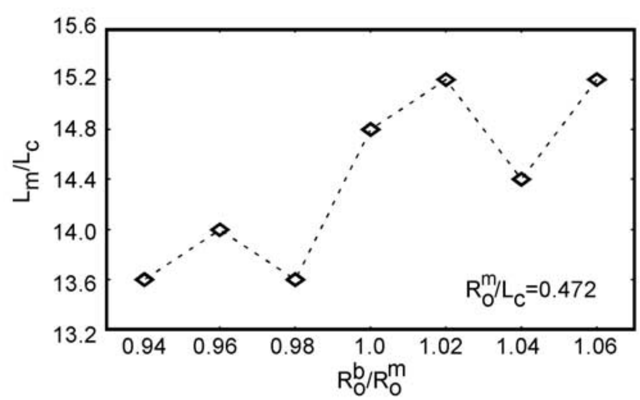

Figure 14. Relation between the nondimensional critical length of the main fault L_m/L_c and static breakdown zone size assumed on each branch R_o^b/R_o^m. The ratio R_o^b/L_c is fixed at 0.472.

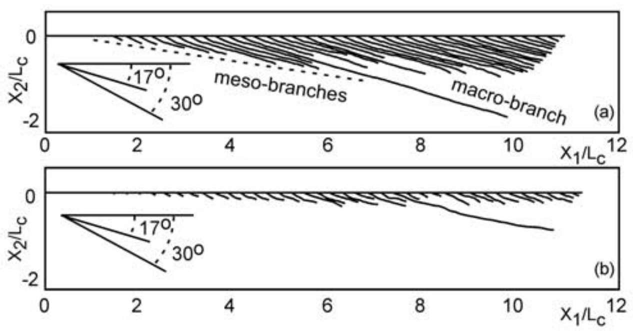

Figure 15. Effects of normal stress on the formation of fault geometry. The normal stress is considered only in Figure 15a. The value $\Delta B/L_c$ = 0.28 is assumed in each example.

of the dependence of τ_p on σ_n in CFM: the extension of the main fault tends to reduce σ_n acting on the branches in CFM since the branches are located on the dilational side of the main fault. The decrease of the absolute value of initial normal stress with increasing clockwise inclination from the growth direction of main fault also makes the peak strength smaller on branches in CFM than in NIM. Second, we observe that the growth direction of the mesobranches and the macrobranches forms a smaller angle with the main fault in NIM than in CFM (about 17°) while the branches begin to grow almost in the same direction (about 30°) in both models soon after their nucleation. These phenomena should occur because the initial stress tends to play more dominant role as the branches extend away from the main fault; in fact, the branches seem to bend toward the direction of initial maximum shear stress in NIM and that of initial maximum CFF_s (about 12° from the direction of the main fault) in CFM. This will be the reason why the growth direction of macrobranch is different in the two models.

[43] What should, however, be emphasized here is the existence of clear qualitative similarity between the two models, in spite of the above slight quantitative differences, in the rupture properties such as the emergence of the macroscopic branch and the linear scaling of the lengths of mesoscopic branches with the length of the main fault. The linear scaling can be understood by the fact that the Coulomb stress is simply a linear superposition of the stresses; it can easily been shown that the normal stress is enhanced in a zone near the tip of the main fault and the zone size increases almost linearly with the extension of the main fault as observed for the shear stress.

[44] We should last note that it is reasonable to expect the qualitatively same result even if we consider the effect of the dynamic normal stress on the residual strength. The reason is quite simple since the extending main fault reduces the residual strength on the branches, which simply makes the branches somewhat larger; this reduction is caused by the decrease in the normal stress acting on the branches.

7.2. Dynamic Complication of Fault Geometry

[45] The emergence of macrobranches, simulated in our study, can contribute to the formation of geometrical complexity of fault system. Our simulations show that interactions between branches trigger the spontaneous growth into macroscopic ones for some of them. Since these interactions are highly nonlinear, it may generally be difficult to precisely predict the nucleation of such macroscopic fault segments. Our calculations, however, indicate that the probability of the emergence of such macrobranch is lower for a main fault with a fixed length when more mesobranches are nucleated as shown in Figure 8. This suggests that the geometry of earthquake fault is simpler when the rock is highly fractured on and near the main fault: the number of nucleated branches may be larger because of higher heterogeneity when the rock is fractured highly. If we can assume that the rock is highly fractured near mature faults, our calculations implies that geometry of mature fault is rather simple. This is the same conclusion as obtained in *Kame and Yamashita* [1999a], although their fault model is significantly different from ours.

[46] Our simulation shows the existence of self-similarity in the geometry of fault structure when the length of the main fault is below the threshold L_{m}. However, such self-similarity is violated once a macrobranch appears. This suggests that there is no simple linear scaling between small and large events. Hence it is also suggested that the behavior of large-size events cannot be predicted from our knowledge about small-size events; the boundary between large-size and small-size events are defined in terms of L_{m} here. It will be studied in our subsequent paper how the breaking of self-similarity is reflected in macroscopic properties of fault.

7.3. Comparison With Previous Related Studies

[47] Some researchers have studied the dynamic growth of a fault taking account of mesoscopic-scale fault structures. For example, *Andrews* [2005] and *Ben-Zion and Shi* [2005] considered the formation of plastic zone as a mesoscopic-scale fault structure near the main fault, while *Yamashita* [2000] assumed the formation of tensile microcracks. It is common in these studies that the mesoscopic fault structure is treated as a bulk and assumed to be a continuous zone. The mesoscopic-scale structure is found to be triangular in all the studies, and self-similarity is observed in the geometry of fault structure; these features are also commonly observed in our present simulations only when the length of the main fault is smaller than a certain threshold. In other words, the distribution of mesoscopic-scale branches can be mimicked by the bulk treatment of mesoscopic-scale fault structure. However, the breaking of self-similarity is never observed in such bulk treatments; it can be observed only when intense interactions between elements in the mesoscopic-scale structure are taken into account.

[48] *Kame and Yamashita* [1999a, 1999b] showed in their numerical analysis that an extending tip of planar fault is bifurcated spontaneously when the fault tip velocity exceeds a certain threshold. They assumed the hoop shear maximization criterion for the growth of fault tip, which is also employed in our present paper for the growth of each branch. They also showed that the dynamic growth of a fault is arrested soon after the bifurcation. It should be noted that the spontaneous bifurcation does not occur for the leading tip of the main fault in our fault model because

the hoop shear traction always takes the maximum on planar direction of the main fault for any fault tip velocity as typically illustrated in Figure 3; our present model rather suggests the possibility of branching behind the leading tip of the main fault (Figure 3). This is largely different from the finding by *Kame and Yamashita* [1999a, 1999b]. This difference occurs because *Kame and Yamashita* [1999a, 1999b] assumed a Griffith-type crack, while we assume here a slip-weakening crack. Since the hoop shear traction is found to shift from the original plane for a high crack tip speed which has the square-root singularity at the extending tip of Griffith type crack, this shifting behavior of traction will disappear in slip-weakening cracks, in which the stress singularity is lower at the crack tip. Comparison of the findings made in this paper and by *Kame and Yamashita* [1999a, 1999b] points out that the behavior of dynamic fault growth is well described by the model studied by *Kame and Yamashita* [1999a, 1999b] if the breakdown zone size is small enough. On the other hand if the breakdown zone size is rather large, our model will be more appropriate and no spontaneous bifurcation of the tip of the main fault is expected. However, it is not easy to investigate numerically the breakdown zone size below which the model of *Kame and Yamashita* [1999a, 1999b] is more appropriate because it is time consuming and requires much computer memory to make simulations assuming small breakdown zone size.

[49] It is finally worth noting that the emergence of macrobranch can be regarded as a typical Hopf bifurcation in term of dynamical system theory [*Hirsch and Smale*, 1974]. *Griffith* [1929] and *Madariaga and Olsen* [2000] showed that an isolated crack begins unstable growth once its length exceeds a certain threshold length for 2-D and 3-D models. It is shown in our present paper that a macrobranch first appears and begins unstable growth when the length of the main fault exceeds L_m, which is dependent on the distribution density of mesobranches and breakdown zone size. This is a distinctive feature of the Hopf bifurcation. However, what makes a striking difference from the models of *Griffith* [1929] and *Madariaga and Olsen* [2000] is that more than one bifurcations can occur for $L > L_m$ in our model.

7.4. Geological Evidence of Branching

[50] Here we discuss the geological evidence for branch generation. Recent detailed field investigations show some evidence of branching of earthquake faults. In fact, *Di Toro et al.* [2005] and *Otsuki et al.* [2003] found the intrusions of melted material into the medium surrounding the principle slip plane. This observation implies that the surrounding medium is ruptured by the dynamic branching of earthquake fault. Although melt intrusions are in general facilitated by tensile ruptures, the existence of high confining pressure at depth suggests that the rupture associated with the melt intrusions will be mixed mode accompanied by shear rupture.

[51] In addition, shear branches are found for several types of natural faults in brittle regime including faults newly formed in intact rocks [*Wilson et al.*, 2005], relatively immature faults [*Di Toro and Pennacchioni*, 2005] and mature faults [*Chester et al.*, 2004]. While the observed branches do not afford direct evidences of *dynamic shear* branching in the latter two cases since they are exhumed, crosscut relations suggests that these branches were formed at a relatively later stage in the recurrence of earthquake ruptures; specifically, for immature faults, some branches overprint neighboring faults accommodating much larger portion of slip [*Di Toro and Pennacchioni*, 2005]. For mature faults, some shear branches off principle slip planes overprint surrounding cataclasite layers [*Chester et al.*, 2004]. Hence it is most likely that these branches are formed during dynamic earthquake rupture.

[52] In addition, field investigations show that some branches exist beyond the cataclasite zone around prominent slip planes or the strain localization zone [*Chester et al.*, 2004; *Di Toro and Pennacchioni*, 2005; *Sowers et al.*, 1994]. It is found that spatial change of fracture strength is rather gradual from a fault core to host rocks [*Lockner et al.*, 2000]. This will facilitate the growth of branches.

[53] All of the above observations strongly support the idea that branches rather easily grow out of the principal fault plane, which is demonstrated and quantitatively modeled in the present study.

7.5. Formation of the Riedel Shear as Mesoscopic-Scale Structure in Brittle Shear Zones

[54] Our simulation result gives an alternative view about the formation mechanism of Riedel shear observed in brittle shear zones, which is regarded as a mesoscopic-scale geological phenomenon. Classical models [*Byerlee*, 1992; *Ramsay and Huber*, 2000; *Tchalenko*, 1970] try to explain it as a progressive strain weakening process of Coulomb-plastic materials: the Riedel shears are formed in the direction close to the maximum compression axis at the initial stage of yielding since the material still has relatively larger values of Coulomb constant (refer to Figure 3.24 of *Scholz* [2002] for the diagram). As the yielding goes on, a prominent shear plane called the Y shear starts to develop in the orientation that is rotated toward the maximum shear load axis from the Riedel shear planes. Once slip is accommodated by the Y shear, the Riedel shears becomes inactive.

[55] Although it might be straightforward to explain the deformation of ductile materials by these classical models at least in the first-order approximation as noted by *Byerlee* [1992], they are inappropriate for the modeling of large deformation of brittle materials since the progress of large deformation of brittle materials ought to be associated with the growth of a large number of small-size ruptures. Note that the classical models do not take account of growth and interactions of such ruptures elements. Our simulation suggests that the Riedel shears, specifically the R_1 shears [e.g., *Byerlee*, 1992], can be explained by dynamically grown mesobranches nucleated on a main rupture plane. It should be noted that the mesobranches are oriented approximately in the direction of maximum compression. The main rupture will correspond to the Y shear: Its orientation is in the direction of maximum shear load in our model. As shown in Figure 3, the main fault tends to grow in the direction of maximum shear load. It is also known that the orientation of Riedel shears is more irregular in brittle shear zones than in ductile shear zones, which can be understood according to our model as being due to dynamic nonlinear interactions between rupture segments.

7.6. Shear Localization Versus Globalization

[56] Evolution of natural faults in the geological timescale usually tends to be considered as a shear localization process due to strain weakening, in which the shear strain is gradually localized into a narrow zone of weakness ending up to a slip plane associated with progressive strain accumulation [e.g., *Ben-Zion and Sammis*, 2003]. The strain localization leads to two important consequences. One is the simplification of fault geometry through the evolution from spatially distributed faults with a variety of lengths to a single dominant fault. The other is that the majority of initially formed small-scale faults become inactive with the fault evolution. Although this view seems to be generally acceptable, our simulation results suggest that the opposite process can also occur in the evolution of some faults.

[57] The present study has shown that dynamic rupture propagation can cause the generation of geometrical complexity of an earthquake fault. In fact, the emergence of macrobranches characterizes the increase in the geometrical complexity of fault; the strain tends to be accommodated over a wider zone with the emergence of macrobranches. This is regarded as the process opposite to the shear localization mentioned above. This process may be termed the shear globalization in contrast with the shear localization.

[58] In nature, the shear globalization will tend to overpass the shear localization when the contrast of strengths at a preexisting weak plane and the host rocks is small enough: the branching is easier to occur when the contrast of strengths is smaller. This will generally be valid not only for a single rupture event in intact medium but also for events occurring on a fault that has experienced many rupture events in its evolution as far as the effect of fault healing is much more significant than that of loading for fault. In fact, detailed geological observations indicate that the above view is appropriate. For example, *Wilson et al.* [2005] observed highly complex geometry of a fault with many branches formed in a single rupture event in a South Africa gold mine. It is also shown that some faults that have experienced many rupture events in their evolution history and have relatively low recurrence rates of earthquakes are also observed to show high geometrical complexity [*Di Toro and Pennacchioni*, 2005]; note that the recurrence rate of earthquakes tends to decrease as the healing effect of fault surpasses the loading effect.

8. Conclusions

[59] We have developed a new hierarchical earthquake rupture model taking account of the mesoscale fault structure, and investigated the dynamic formation of fault geometry and its effects on dynamic earthquake rupture process. We have assumed the nucleation of branches on the main fault. As long as the length of main fault is below a certain threshold L_{m}, the spontaneous growths of these branches are arrested soon, and the arrested branches form a self-similar geometrical structure. This suggests that there is a simple scaling between small and large events as long as the length of the main fault is smaller than L_m. However, the fluctuation in the lengths of branches becomes conspicuous with the growth of the main fault; this fluctuation is caused by the intense nonlinear interactions between branches and heterogeneous or discrete nature of our fault model. Heterogeneity is a general feature of fault material; therefore this phenomenon would be expected in nature. The amplitude of fluctuation is shown to increase rapidly, and a branch begins unstable growth and appears as a macroscopic fault segment once the length of the main fault exceeds L_m. This indicates that the above mentioned scaling relation is never valid between events whose fault lengths are below and above L_m. Our study also suggests the critical importance of consideration of mesoscopic-scale fault structure in understanding the dynamics of earthquakes; mesoscopic scale fault structures play a key role in producing dynamically macroscopic rupture phenomena such as generation of macroscopic branches and the rupture velocity of main fault. Once macroscopic-scale branches are formed, they will further affect the rupture processes. It should also be noted that the finding of the breaking of scaling is attributable to our unique modeling of off main fault damage, which is represented by multiple interactive rupture segments (not a bulk continuous zone).

[60] **Acknowledgments.** This paper benefited from thoughtful reviews by Associate Editor, N. Kame, and an anonymous reviewer. The authors also appreciate helpful comments by B. E. Shaw for the manuscript. R. A. is supported by Japan Society for Promotion of Science (JSPS) Postdoctoral fellowship in 2005–2007. The work was additionally supported by the "DaiDaiToku" Project, MEXT, Japan.

References

Aki, K., and P. G. Richards (2002), *Quantitative Seismology*, 2nd ed., 700 pp., Univ. Sci. Books, Sausalito, Calif.
Ando, R. (2005), Development of efficient spatio-temporal boundary integral equation method and theoretical study on dynamics of fault zone formation and earthquake ruptures (in Japanese), Univ. of Tokyo, Tokyo.
Ando, R., T. Tada, and T. Yamashita (2004), Dynamic evolution of a fault system through interactions between fault segments, *J. Geophys. Res.*, *109*, B05303, doi:10.1029/2003JB002665.
Ando, R., N. Kame, and T. Yamashita (2007), An efficient boundary integral equation method applicable to the analysis of non-planar fault dynamics, *Earth Planets Space*, *59*, 363–373.
Andrews, D. J. (1976a), Rupture propagation with finite stress in antiplane strain, *J. Geophys. Res.*, *81*, 3575–3582.
Andrews, D. J. (1976b), Rupture velocity of plane strain shear cracks, *J. Geophys. Res.*, *81*, 5679–5687.
Andrews, D. J. (2005), Rupture dynamics with energy loss outside the slip zone, *J. Geophys. Res.*, *110*, B01307, doi:10.1029/2004JB003191.
Aochi, H., and E. Fukuyama (2002), Three-dimensional nonplanar simulation of the 1992 Landers earthquake, *J. Geophys. Res.*, *107*(B2), 2035, doi:10.1029/2000JB000061.
Archuleta, R. J. (1984), A faulting model for the 1979 Imperial Valley earthquake, *J. Geophys. Res.*, *89*, 4559–4585.
Ben-Zion, Y., and J. R. Rice (1995), Slip patterns and earthquake populations along different classes of faults in elastic solids, *J. Geophys. Res.*, *100*, 12,959–12,983.
Ben-Zion, Y., and C. G. Sammis (2003), Characterization of fault zones, *Pure Appl. Geophys.*, *160*(3–4), 677–715.
Ben-Zion, Y., and Z. Q. Shi (2005), Dynamic rupture on a material interface with spontaneous generation of plastic strain in the bulk, *Earth Planet. Sci. Lett.*, *236*(1–2), 486–496.
Byerlee, J. (1992), The change in orientation of subsidiary shears near faults containing pore fluid under high-pressure, *Tectonophysics*, *211*(1–4), 295–303.
Chester, F. M., and D. L. Kirschner (2000), Geochemical investigation of fluid involvement in exhumed faults of the San Andreas system, National Earthquake Hazards Reduction Program, in *Annual Project Summary*, vol. 41, U.S. Geol. Surv., Reston, Va.
Chester, F. M., J. S. Chester, D. L. Kirschner, S. E. Schulz, and J. P. Evans (2004), Structure of large-displacement, strike-slip fault zones in the brittle continental crust, in *Rheology and Deformation of the Lithosphere at Continental Margins*, edited by G. D. Karner et al., pp. 223–261, Columbia Univ. Press, New York.
Cochard, A., and R. Madariaga (1994), Dynamic faulting under rate-dependent friction, *Pure Appl. Geophys.*, *142*(3–4), 419–445.

Dalguer, L. A., K. Irikura, and J. D. Riera (2003), Simulation of tensile crack generation by three-dimensional dynamic shear rupture propagation during an earthquake, *J. Geophys. Res.*, *108*(B3), 2144, doi:10.1029/2001JB001738.

Di Toro, G., and G. Pennacchioni (2005), Fault plane processes and mesoscopic structure of a strong-type seismogenic fault in tonalites (Adamello batholith, Southern Alps), *Tectonophysics*, *402*(1–4), 55–80.

Di Toro, G., S. Nielsen, and G. Pennacchioni (2005), Earthquake rupture dynamics frozen in exhumed ancient faults, *Nature*, *436*(18), 1009–1012.

Dieterich, J. H. (1979), Modeling of rock friction: 1. Experimental results and constitutive equations, *J. Geophys. Res.*, *84*, 2161–2168.

Dieterich, J. H., and B. D. Kilgore (1994), Direct observation of frictional contacts: New insights for state-dependent properties, *Pure Appl. Geophys.*, *143*(1–3), 283–302.

Fukuyama, E., W. L. Ellsworth, F. Waldhauser, and A. Kubo (2003), Detailed fault structure of the 2000 western Tottori, Japan, earthquake sequence, *Bull. Seismol. Soc. Am.*, *93*(4), 1468–1478.

Griffith, A. A. (1929), The phenomenon of rupture and flow in solids, *Philos. Trans. R. Soc. London, Ser. A*, *221*, 163–198.

Hirsch, M. W., and S. Smale (1974), *Differential Equations, Dynamical Systems, and Linear Algebra*, 358 pp., Academic, New York.

Ida, Y. (1972), Cohesive force across the tip of a longitudinal-shear crack and Griffith's specific surface energy, *J. Geophys. Res.*, *77*, 3796–3805.

Ide, S., and M. Takeo (1997), Determination of constitutive relations of fault slip based on seismic wave analysis, *J. Geophys. Res.*, *102*, 27,379–27,391.

Kame, N., and T. Yamashita (1999a), A new light on arresting mechanism of dynamic earthquake faulting, *Geophys. Res. Lett.*, *26*, 1997–2000.

Kame, N., and T. Yamashita (1999b), Simulation of the spontaneous growth of a dynamic crack without constraints on the crack tip path, *Geophys. J. Int.*, *139*(2), 345–358.

Kame, N., and T. Yamashita (2003), Dynamic branching, arresting of rupture and the seismic wave radiation in self-chosen crack path modelling, *Geophys. J. Int.*, *155*(3), 1042–1050.

Kame, N., J. R. Rice, and R. Dmowska (2003), Effects of prestress state and rupture velocity on dynamic fault branching, *J. Geophys. Res.*, *108*(B5), 2265, doi:10.1029/2002JB002189.

Kanamori, H., and T. Heaton (2000), Microscopic and macroscopic physics of earthquakes, in *GeoComplexity and the Physics of Earthquakes*, *Geophys. Monogr. Ser.*, vol. 120, edited by J. R. Rundle, D. L. Turcotte, and W. Klein, pp. 147, AGU, Washington, D. C.

Kim, Y.-S., D. C. P. Peacock, and D. J. Sanderson (2004), Fault damage zones, *J. Struct. Geol.*, *26*(3), 503–517.

Koller, M. G., M. Bonnet, and R. Madariaga (1992), Modeling of dynamic crack-propagation using time-domain boundary integral-equations, *Wave Motion*, *16*(4), 339–366.

Kostrov, B. V. (1964), Self-similar problems of propagation of shear cracks, *J. Appl. Math. Mech.*, *28*, 1077–1087.

Lockner, D. A., H. Naka, H. Tanaka, H. Ito, and R. Ikeda (2000), Permeability and strength of core samples from the Nojima Fault of the 1995 Kobe earthquake, in *Proceedings of the International Workshop on the Nojima Fault Core and Borehole Data Analysis*, *U.S. Geol. Surv. Open File Rep.*, *129*, 147–152.

Lyakhovsky, V., Y. Ben-Zion, and A. Agnon (1997), Distributed damage, faulting, and friction, *J. Geophys. Res.*, *102*, 27,635–27,649.

Madariaga, R., and K. B. Olsen (2000), Criticality of rupture dynamics in 3-D, *Pure Appl. Geophys.*, *157*(11–12), 1981–2001.

Marone, C. (1998), Laboratory-derived friction laws and their application to seismic faulting, *Annu. Rev. Earth Planet. Sci.*, *26*, 643–696.

Marone, C., C. B. Raleigh, and C. H. Scholz (1990), Frictional behavior and constitutive modeling of simulated fault gouge, *J. Geophys. Res.*, *95*, 7007–7025.

Moore, D. E., and D. A. Lockner (1995), The role of microcracking in shear-fracture propagation in granite, *J. Struct. Geol.*, *17*(1), 95–114.

Nakanishi, A., N. Takahashi, J. Park, S. Miura, S. Kodaira, Y. Kaneda, N. Hirata, T. Iwasaki, and M. Nakamura (2002), Crustal structure across the coseismic rupture zone of the 1944 Tonankai earthquake, the central Nankai Trough seismogenic zone, *J. Geophys. Res.*, *107*(B1), 2007, doi:10.1029/2001JB000424.

Ohnaka, M. (2003), A constitutive scaling law and a unified comprehension for frictional slip failure, shear fracture of intact rock, and earthquake rupture, *J. Geophys. Res.*, *108*(B2), 2080, doi:10.1029/2000JB000123.

Ohnaka, M., and Y. Kuwahara (1990), Characteristic features of local breakdown near a crack-tip in the transition zone from nucleation to unstable rupture during stick-slip shear failure, *Tectonophysics*, *175*(1–3), 197–220.

Olsen, K. B., R. Madariaga, and R. J. Archuleta (1997), Three-dimensional dynamic simulation of the 1992 Landers earthquake, *Science*, *278*(5339), 834–838.

Otsuki, K., N. Monzawa, and T. Nagase (2003), Fluidization and melting of fault gouge during seismic slip: Identification in the Nojima fault zone and implications for focal earthquake mechanisms, *J. Geophys. Res.*, *108*(B4), 2192, doi:10.1029/2001JB001711.

Palmer, A. C., and J. R. Rice (1973), Growth of slip surfaces in progressive failure of over-consolidated clay, *Proc. R. Soc. London, Ser. A*, *332*(1591), 527–548.

Peyrat, S., K. Olsen, and R. Madariaga (2001), Dynamic modeling of the 1992 Landers earthquake, *J. Geophys. Res.*, *106*, 26,467–26,482.

Poliakov, A. N. B., R. Dmowska, and J. R. Rice (2002), Dynamic shear rupture interactions with fault bends and off-axis secondary faulting, *J. Geophys. Res.*, *107*(B11), 2295, doi:10.1029/2001JB000572.

Ramsay, J. G., and I. H. Huber (2000), *The Techniques of Modern Structural Geology*, 1061 pp., Academic, London.

Rice, J. R. (1980), The mechanics of earthquake rupture, in *Physics of the Earth's Interior*, edited by A. M. Dziewonski and E. Boschi, pp. 555–649, North-Holland, Amsterdam, Netherlands.

Rice, J. R., C. G. Sammis, and R. Parsons (2005), Off-fault secondary failure induced by a dynamic slip-pulse, *Bull. Seismol. Soc. Am.*, *95*, 109–134.

Ruina, A. (1983), Slip instability and state variable friction laws, *J. Geophys. Res.*, *88*, 359–370.

Scholz, C. H. (2002), *The Mechanics of Earthquakes and Faulting*, 2nd ed., 471 pp., Cambridge Univ. Press, Cambridge, U. K.

Scholz, C. H., N. H. Dawers, J. Z. Yu, and M. H. Anders (1993), Fault growth and fault scaling laws: Preliminary results, *J. Geophys. Res.*, *98*, 21,951–21,961.

Sowers, J. M., J. R. Unruh, W. R. Lettis, and T. D. Rubin (1994), Relationship of the Kickapoo fault to the Johnson Valley and Homestead Valley faults, San Bernardino County, California, *Bull. Seismol. Soc. Am.*, *84*(3), 528–536.

Tada, T., and R. Madariaga (2001), Dynamic modelling of the flat 2-D crack by a semi-analytic BIEM scheme, *Int. J. Numer. Methods Eng.*, *50*(1), 227–251.

Tada, T., and T. Yamashita (1997), Non-hypersingular boundary integral equations for two-dimensional non-planar crack analysis, *Geophys. J. Int.*, *130*(2), 269–282.

Tchalenko, J. S. (1970), Similarities between shear zones of different magnitudes, *Geol. Soc. Am. Bull.*, *81*(6), 1625–1639.

Tchalenko, J. S., and M. Berberian (1975), Dasht-E Bayaz Fault, Iran: Earthquake and earlier related structures in bed rock, *Geol. Soc. Am. Bull.*, *86*(5), 703–709.

Vermilye, J. M., and C. H. Scholz (1998), The process zone: A microstructural view of fault growth, *J. Geophys. Res.*, *103*, 12,223–12,237.

Wilson, B., T. Dewers, Z. Reches, and J. Brune (2005), Particle size and energetics of gouge from earthquake rupture zones, *Nature*, *434*(7034), 749–752.

Xia, K. W., A. J. Rosakis, and H. Kanamori (2004), Laboratory earthquakes: The sub-Rayleigh-to-supershear rupture transition, *Science*, *303*(5665), 1859–1861.

Yamashita, T. (1998), Simulation of seismicity due to fluid migration in a fault zone, *Geophys. J. Int.*, *132*(3), 674–686.

Yamashita, T. (2000), Generation of microcracks by dynamic shear rupture and its effects on rupture growth and elastic wave radiation, *Geophys. J. Int.*, *143*(2), 395–406.

R. Ando, National Research Institute for Earth Science and Disaster Prevention, 3-1 Tennodai, Tsukuba, Ibaraki 305-0006, Japan. (ando@bosai.go.jp)

T. Yamashita, Earthquake Research Institute, University of Tokyo, 1-1-1 Yayoi, Bunkyo-ku, Tokyo 113-0032, Japan.